Spectrochimica Acta Part A: Molecular and Biomolecular Spectroscopy 151 (2015) 156–163

Contents lists available at ScienceDirect

Spectrochimica Acta Part A: Molecular and Biomolecular Spectroscopy

journal homepage: www.elsevier.com/locate/saa

EXAFS and DFT study of the cadmium and lead adsorption on modified silica nanoparticles

Valeria B. Arce [a,b], Romina M. Gargarello [a], Florencia Ortega [a], Virginia Romañano [a], Martín Mizrahi [a], José M. Ramallo-López [a], Carlos J. Cobos [a], Claudio Airoldi [c], Cecilia Bernardelli [d], Edgardo R. Donati [d], Daniel O. Mártire [a,*]

[a] Instituto de Investigaciones Fisicoquímicas Teóricas y Aplicadas (INIFTA), CCT-La Plata-CONICET, Universidad Nacional de La Plata, Diag 113 y 64, 1900 La Plata, Argentina
[b] Centro de Investigaciones Ópticas (CIOp), CONICET La Plata-CIC, CC 3, 1897 Gonnet, La Plata, Argentina
[c] Chemistry Institute, University of Campinas, P.O. Box 6154, 13084-971 Campinas, São Paulo, Brazil
[d] Centro de Investigación y Desarrollo en Fermentaciones Industriales, CINDEFI (CCT La Plata-CONICET, Universidad Nacional de La Plata), Facultad de Ciencias Exactas, 50 y 115, 1900 La Plata, Argentina

HIGHLIGHTS

- Modified silica nanoparticles were prepared and characterized by FTIR and ^{13}C NMR.
- Isotherms for the adsorption of Cd^{2+} and Pb^{2+} ions on the particles were obtained.
- Pb–N and Pb–C distances on the particles were obtained by EXAFS.
- DFT calculations supported the experimental data.
- Hybrid nanoparticles by precipitation allowed the easy removal of the nano-sorbents.

GRAPHICAL ABSTRACT

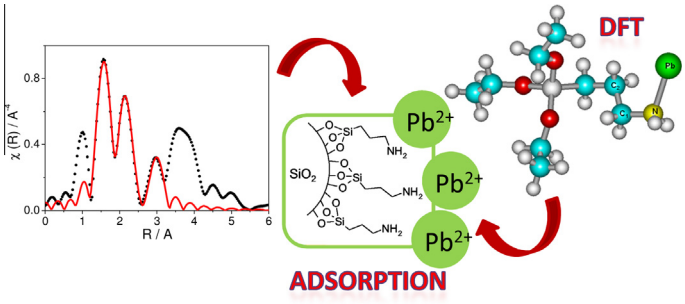

ARTICLE INFO

Article history:
Received 31 March 2015
Received in revised form 17 June 2015
Accepted 18 June 2015
Available online 24 June 2015

Keywords:
Cadmium
Lead
Silica nanoparticles
EXAFS
DFT
MEH-PPV

ABSTRACT

Silica nanoparticles of 7 nm diameter were modified with (3-aminopropyl) triethoxysilane (APTES) and characterized by CP-MAS ^{13}C and ^{29}Si NMR, FTIR, zeta potential measurements, and thermogravimetry. The particles were shown to sorb successfully divalent lead and cadmium ions from aqueous solution. Lead complexation with these silica nanoparticles was clearly confirmed by EXAFS (Extended X-ray Absorption Fine Structure) with synchrotron light measurements. Predicted Pb–N and Pb–C distances obtained from quantum-chemical calculations are in very good agreement with the EXAFS determinations. The calculations also support the higher APTES affinity for Pb^{2+} compared to Cd^{2+}.

1. Introduction

Effluents from industrial applications including mining, refining and production of textiles, paints and dyes may contain heavy metal ions at high concentrations [1]. In particular, lead and

* Corresponding author.
E-mail address: dmartire@inifta.unlp.edu.ar (D.O. Mártire).

http://dx.doi.org/10.1016/j.saa.2015.06.093
1386-1425/

cadmium are considered priority metals in the framework of the European water policy (Directive 2013/39/EU [2]), because they present a significant risk to biota and humans, given its persistence, toxicity and bioaccumulation characteristics.

A wide variety of techniques to remove heavy metals from water is available, such as ion exchange, reverse osmosis and nanofiltration, precipitation, coagulation/co-precipitation and sorption [3]. Among them, adsorption is considered as one of the most suitable methods due to its ease of operation and the availability of a wide range of adsorbents. Organofunctionalization of adsorbents for the removal of heavy metal ions from water has attracted great research interest in the last decade due to the advantages of achieving high efficiency and good selectivity [4,5]. In particular, amines have been used to functionalize silica [5] to synthesize sorbents for heavy metal ions removal from aqueous media. Mesoporous silica materials chemically modified with aminopropyl, [2-aminoethylamino]-propyl, and [(2-aminoethyla mino)-ethylamino]-propyl [6] were recently employed to sorb divalent copper, nickel, lead, cadmium and zinc from aqueous solution.

In this context we here prepared 7 nm-diameter silica nanoparticles organofunctionalized with aminopropyl groups to sorb divalent lead and cadmium ions from aqueous solution. Sorption isotherms for these cations on the silica particles were favorably obtained. Complexation of Pb^{2+} with the silica nanoparticles was confirmed by EXAFS (Extended X-ray Absorption Fine Structure) with synchrotron light measurements. To compare predicted Pb–N and Pb–C distances in the modified nanoparticles bonded to Pb^{2+} with the EXAFS determinations, quantum-chemical calculations were carried out.

Separation of small silica nanoparticles by filtration or ultracentrifugation can be a cumbersome procedure. Thus, to facilitate the separation of the nanomaterial by filtration, after sorption of the metal ions an alternative novel method involving the synthesis of bigger composite particles (NPNH2@MEH-PPV) of the copolymer poly[2-methoxy-5-(2-ethylhexyl-oxy)-1,4-phenylene-vinylene] (MEH-PPV, Fig. 1a) and the modified silica nanoparticles was employed here.

2. Materials and methods

2.1. Materials

Fumed silica (Sigma, specific surface area; SSA = (390 ± 40) $m^2\ g^{-1}$, particle diameter estimated from the SSA = 7 nm and confirmed by TEM images [7]), toluene (Baker, p.a.), ethyl acetate (Ciccarelli, p.a.), CaH_2 (Fluka), $Pb(NO_3)_2$ (Timper), tetrahydrofurane (THF) Biopack, and $CdSO_4{\cdot}8/3H_2O$, $CaCl_2$, (3-aminopropyl) triethoxysilane (APTES) and poly[2-methoxy-5-(2-ethylhexyl-oxy)-1,4-phenylene-vinylene] (MEH-PPV) from Sigma–Aldrich were used without further purification. Distilled water (>18 MΩ cm^{-1}, <20 μg L^{-1} organic carbon) was obtained from a Millipore (Bedford, MA) system.

2.2. Modification and characterization of silica nanoparticles

Commercial fumed silica was first dried for 15 h at 150 °C. Activation of silanol groups was subsequently achieved by heating at 250 °C for 3 h. Modified silica nanoparticles were synthesized by a variation of the method published by Foscheira et al. [6]. Briefly, 1.0 g of previously dried and activated silica was mixed with 80 mL of toluene and 1.5 mL of (3-aminopropyl) triethoxysilane. The mixture was heated and maintained under reflux (110–120 °C) for 48 h. To preserve a dry environment a guard tube filled with calcium chloride was connected to the reflux condenser. Modified nanoparticles (from now named NPNH2) were recovered by evaporating the reaction solvent (toluene), washing gently with ethyl acetate, filtering through 0.22 μm nylon membrane (Osmonics Inc.) and drying at 0.1 Torr for 5 h.

The conditions of the CP-MAS ^{13}C and ^{29}Si nuclear magnetic resonance (NMR) experiments were described elsewhere [7].

The zeta potential measurements (0.5 g L^{-1} water suspension at constant ionic strength of 10^{-3} M KCl) were performed at 25.0 ± 0.1 °C with a Brookhaven 90Plus/Bi-MAS instrument, operating at λ = 635 nm from a 15 mW-solid state laser.

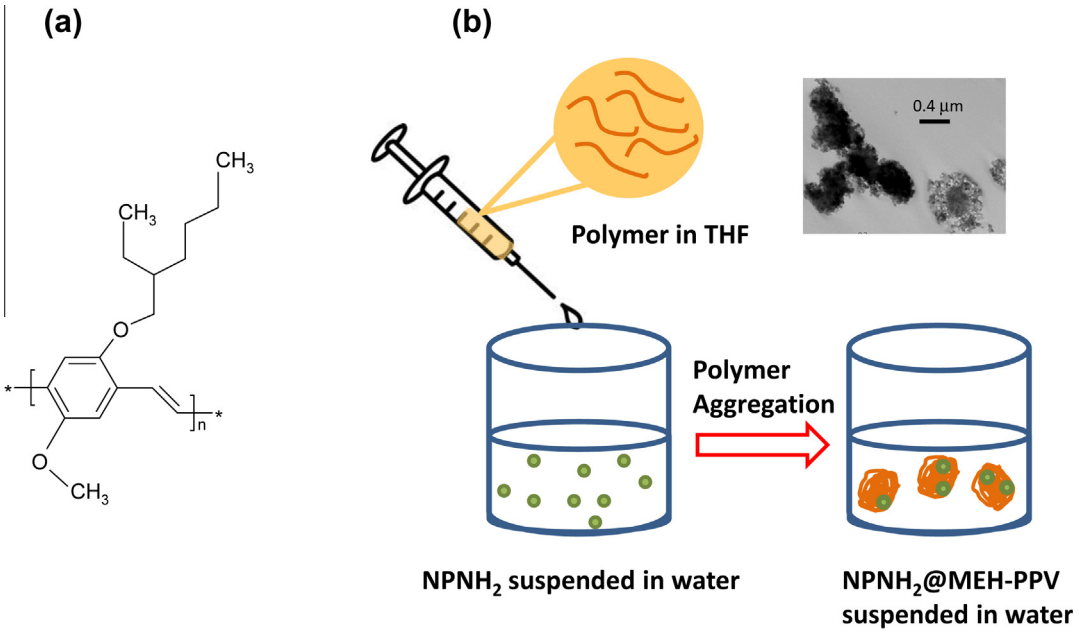

Fig. 1. (a) Molecular formula of MEH-PPV. (b) Synthesis of NPNH2@MEH-PPV. Inset: TEM images of the hybrid NPNH2@MEH-PPV nanoparticles.

For the FTIR measurements a Varian 660 spectrometer equipped with a DTGS detector was employed. The spectra were acquired in the transmission mode with a spectral resolution of 4 cm^{-1} accumulating 128 scans.

The thermogravimetric curve was performed with a DuPont Model 951 instrument, under Ar atmosphere with heating rate of 0.17 K s^{-1}. The instrument was calibrated with $CaC_2O_4{\cdot}3H_2O$.

Nitrogen analysis was performed by catalytic combustion with a Thermo Finnigan, CE Flash EA 1112 elemental analyzer.

The specific surface area (SSA) was evaluated by means of the Brunauer–Emmett–Teller (BET) equation applied to nitrogen adsorption isotherms as reported elsewhere [8].

2.3. Batch sorptions

A series of plastic vials containing solution of 1.0 g L^{-1} of NPNH2 were incubated overnight at 25.0 ± 0.1 °C with aqueous solutions of different concentration of Pb^{2+} (pH = 3) or Cd^{2+} (pH = 6) in a reciprocal shaker at 150 rpm. The content of each vial was then filtered through a 0.1 μm membrane. The final metal concentration was determined in the filtered solution by atomic absorption spectrophotometry (Shimadzu AA6650, Shimadzu Corporation Kyoto, Japan).

The metal uptake capacity, Q, was calculated from the difference between the initial (C_i) and equilibrium (C_{eq}) concentrations as shown in Eq. (1).

$$Q = \frac{(C_i - C_{eq})V}{M} \quad (1)$$

where, Q (mmol/g) is the sorbed metal quantity per gram of sorbent at any time, M (g) is the sorbent dosage, and V (L) is the solution volume.

2.4. Synthesis of the hybrid nanoparticles NPNH2@MEH-PPV

Multiphase particles of the copolymer MEH-PPV (Fig. 1a) and the modified silica nanoparticles containing the metal ions were prepared by a controlled precipitation method [9,10]. The procedure is based on a controlled precipitation of the polymer in aqueous medium (see Fig. 1b). Briefly, a 0.5 g L^{-1} stock solution of the polymer was prepared in tetrahydrofuran (THF). A volume of 0.5 mL of the stock solution was added to 10 mL of aqueous solutions containing 0.25 mg of NPNH2 and different concentration of Pb^{2+} (pH = 3) or Cd^{2+} (pH = 6), preincubated for 4 h at 25.0 °C in a reciprocal shaker at 150 rpm. The content of each vial was then filtered through a 0.1 μm membrane. Final metal concentration was determined in the filtrate solution by atomic absorption. Particle formation occurs by precipitation of the polymer upon rapidly adding the polymer solution to an excess of the aqueous phase [9,10].

2.5. XAFS measurements

Lead L_3-edges XAFS spectra were measured at the XAFS2 beam line at the Laboratorio Nacional de Luz Síncrotron (LNLS, Campinas, Brazil) at room temperature in transmission mode with three ion chambers as detectors. The third one was used to measure the metallic reference simultaneously with the sample. Powder sample was pressed in a pellet optimizing the absorption step and total absorption. The EXAFS (Extended X-ray Absorption Fine Structure) oscillations $\chi(k)$ was extracted from the experimental data with standard procedures using the Athena program, part of the IFEFFIT package [11]. The Fourier transformation was calculated using the Hanning filtering function. The k^3-weighted $\chi(k)$ data, to enhance the oscillations at higher k, were Fourier transformed. EXAFS modeling was carried out using the ARTEMIS program which is also part of the IFFEFIT package. Structural parameters (coordination numbers and bond lengths and their mean squared disorders) were obtained by a nonlinear least-squares fit of the theoretical EXAFS signal to the data in R space by Fourier transforming both the theory and the data. Theoretical scattering path amplitudes and phase shifts for all paths used in the fits were calculated using the FEFF6 code [12]. The k-range was set from 2.5 to 12 $Å^{-1}$, the Fourier transforms were fitted in region 1.2–3.2 Å and the fits were performed simultaneously to k, k^2 and k^3-weighted data. The passive reduction factor S_0^2 was restrained to values of 0.7. This value was obtained from fitting of metallic Pb foil standard by constraining the coordination number in this compound of known crystal structure.

2.6. Density functional theory calculations

To compare predicted Pb–N and Pb–C distances in the APTES-functionalized nanoparticles bonded to Pb^{2+} with the EXAFS determinations, quantum-chemical calculations were carried out. The popular density functional hybrid method B3LYP [13–15] and the hybrid meta-generalized exchange–correlation functional M06-2X [16] combined with the CEP-121G basis set [17,18] were employed. In the CEP-121G, compact effective potentials (CEP) replace the atomic core electrons, while the valence pseudo-orbitals are described by Gaussian expansions with a triple-zeta contraction scheme (triple-split valence basis set). In particular for APTES–Pb^{2+} calculations, the 44 alpha electrons and the 44 beta electrons are distributed in molecular orbitals which comprise 245 basis functions based on 359 primitive Gaussians. In comparative calculations for PTES-Cd^{2+} the 52 alpha electrons and the 52 beta electrons are distributed in molecular orbitals which comprise 271 basis functions based on 401 primitive Gaussians. Bulk hydratation effects were considered using the conductor-like polarizable continuum model, CPCM [19]. Molecular geometry optimizations without symmetry constraints were performed using analytical gradient methods. To derive thermodynamic properties, the harmonic vibrational frequencies were then derived via analytical second derivative methods. All calculations were performed with the Gaussian 09 program package [20].

3. Results and discussion

3.1. Characterization of NPNH2

3.1.1. Infrared spectroscopy

The FTIR spectrum of NPNH2 shows additional peaks compared to those reported for bare silica nanoparticles [7,21] (see Fig. 2 and

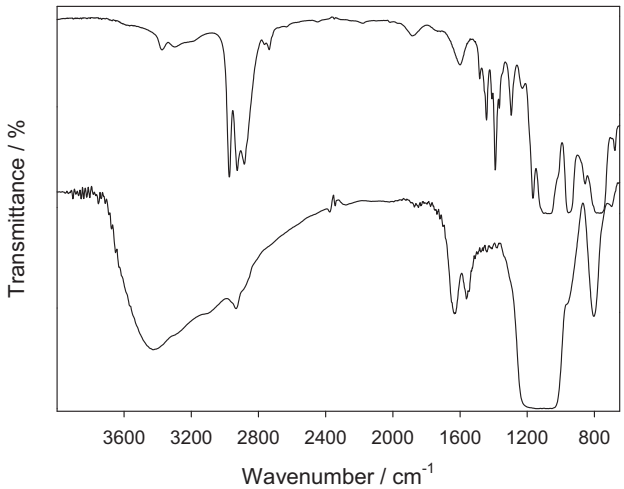

Fig. 2. FTIR spectra of: NPNH2 (lower trace) and APTES (upper trace).

Table 1
Bands observed in FTIR spectra of APTES and NPNH2.

APTES	NPNH2
2926.5	2932.1
2973.0	2962.2 (h)
2883.3	2882.1 (h)
1442.3	1440.4
1410.4	1409.7
1389.7	1382.1
1365.2	1365.5

Table 1). These bands are also present in the spectrum of APTES. The bands in the 3000–2800 cm^{-1} region are assigned to the CH_2 stretching [22]. Absorption bands in the region 1575–1450 cm^{-1} may be assigned to N–H vibrations in protonated amines [23]. The N–H stretch absorption over the 3300–3400 cm^{-1} present in APTES [24] is masked by the O–H absorption present in silica [21]. Any absorption due to the vibration modes assigned to the Si—O—C moiety is shrouded by the strong Si—O—Si absorption signals at 1100 cm^{-1} [22]. Absorption at 1332 and 1630 cm^{-1} was assigned to CO_2 trapped by surface NH_3^+ giving rise to an amine bicarbonate moiety in coincidence with that reported for protonated (3-aminopropyl) triethoxysilane films and aged silicon particles modified with propylamine groups [25].

The percentage of organic groups (%OG = 9.8%) for NPNH2 was estimated from the loss of mass observed from 200 to 700 °C in the TG analysis (see TG curve in Fig. S1 of the Electronic Supplementary material). This value is in excellent agreement with the 1.04 ± 0.02% N content determined by nitrogen analysis. The specific surface area (SSA) of the bare SiO_2 nanoparticles employed in the synthesis of NPNH2 is 390 ± 40 $m^2 g^{-1}$. The value of SSA = 148.4 ± 0.7 $m^2 g^{-1}$ was obtained here by application of the BET method to NPNH2. The decrease in specific surface area upon silica functionalization with the organic groups was already reported for different systems [7].

The previous data confirm the existence of APTES on the surface of the silica nanoparticles. The presence of amino groups on the silica surface was also confirmed by the ninhydrin assay [26].

In order to investigate the bonding between APTES and silica, NMR spectra of ^{13}C and ^{29}Si nuclei in solid phase were obtained.

The solid-state ^{13}C MAS NMR spectrum presented in Fig. 3(a) provides fundamental information regarding the nature of the aminopropyl groups grafted on the surface of the silica particles. Three well-resolved peaks observed at 10, 23 and 43 ppm are assigned to the C1, C2 and C3 carbons of the incorporated aminopropyl groups, respectively, as indicated by the numbered structure inserted [27,28]. The presence of these signals infers that the structure of the aminopropyl groups remains intact after the incorporation reaction. The absence of peaks related to residual ethoxy carbons, which would appear around 18 and 60 ppm in the spectrum, suggests that the hydrolysis and/or condensation of the silane (3-aminopropyl) trialkoxysilane molecules on the surface of the silica nanoparticles was practically complete [29].

The ^{29}Si NMR spectrum of the silica nanoparticles organofunctionalized with aminopropyl groups, shown in Fig. 3(b), presents intense broad signals at −108 and −99 ppm that can be assigned to $Si(OSi)_4$ structural units, also referred as Q^4 species, and $Si(OSi)_3OH$ units, also known as Q^3 species, respectively. Q^4 structural units represent interlinked SiO_4 tetrahedrons in the interior of silica framework, while Q^3 sites are present on the surface associated with silanol groups [29]. Furthermore, another two peaks at −67 and −58 ppm are observable due to the incorporation of aminopropyl groups on the surface. Also, no signal is noticeable around −45 ppm, which would correspond to the chemical shift of silicon atoms in liquid (3-aminopropyl) trialkoxysilane, indicating the absence of free silane molecules physically sorbed on the silica surface.

The grafting of organic species onto the silica surface leads to the appearance of peaks at −67 and −58 ppm in the spectrum, indicating the generation of new siloxane linkages (Si—O—Si) of the aminopropylsilane silicon to the surface silicon atoms of the silica nanoparticles. The signal at −67 ppm is attributed to the aminopropylsilane silicon attached to the surface of the material via three siloxane bonds, $(-O-)_3Si-R$ (T^3; where R = aminopropyl chain), while the peak at −58 ppm is attached via two siloxane bonds, $(-O-)_2Si(OH)R$ (T^2). The relative high intensity of T^2 and T^3 species and the absence of T^1 species [$(-O-)Si(OH)_2R$] indicate that the incorporated aminopropyl groups are closely packed on the surface of the material through tridentate and bidentate linkages instead of a monodentate one [29,30].

It can be seen from the dependence of the zeta potential of the NPNH2 dispersion on pH (Fig. 4) that the pH of the zero point of charge (PZC), i.e., the pH where the zeta potential equals zero, is 9.15. At pH below 9.15, the particles charge is positive due to the protonation of the amino-modification compensating the negative charge of the silanol groups. These groups are responsible for the PZC of bare silica, which is between pH 1 and 2, depending on the particle size [31,32]. For the NPNH2 in suspensions of pH above 9.15, where several of the amino groups are not protonated (pKa of

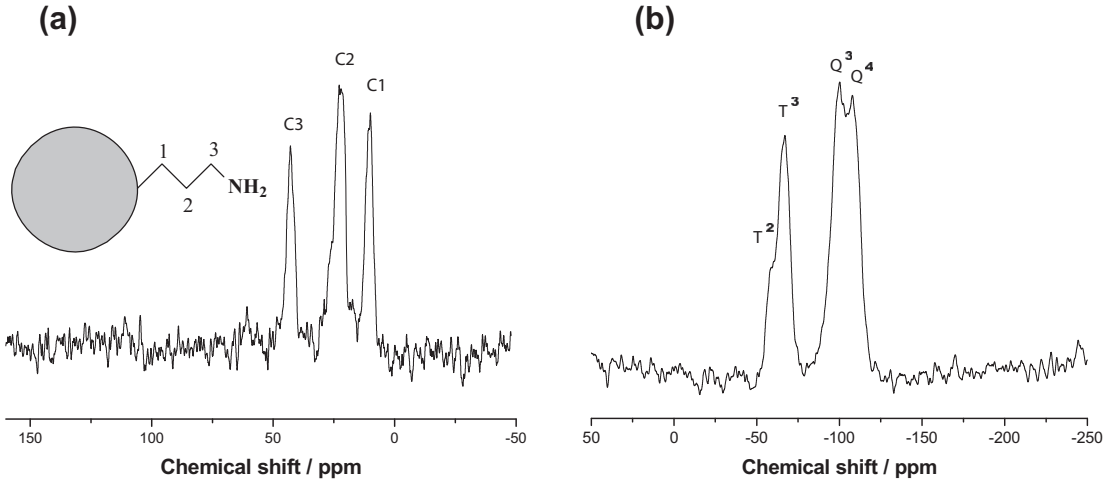

Fig. 3. Solid-state NMR spectrum of the amino-functionalized silica nanoparticles: ^{13}C (a) and ^{29}Si (b).

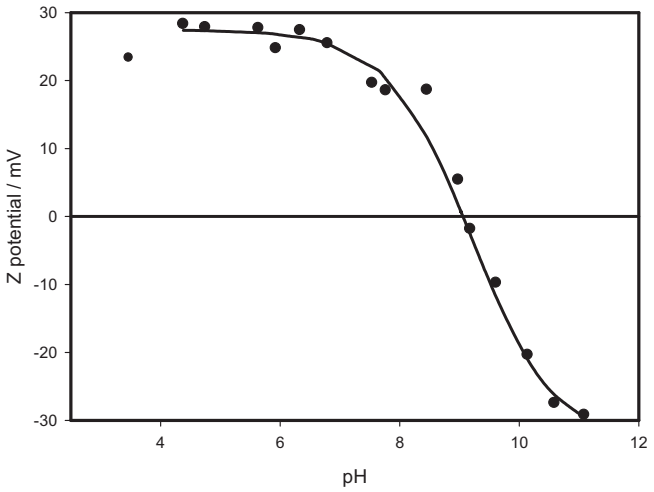

Fig. 4. Dependence of zeta potential of the NPNH2 suspensions on pH.

free propylamine = 10.566 [33]), the particles possess negative zeta potentials. The values of zeta potential obtained at pH below 4 are underestimated because the ionic strength cannot be considered constant in the medium containing 0.001 M KCl.

3.2. Batch sorption experiments

The amount of sorbed metal Q from 100 mg L^{-1} solutions of Cd^{2+} or Pb^{2+} reached constant values after 4 h of incubation. Thus, to assure equilibrium conditions in the batch sorption experiments the systems were incubated overnight. The percentage of sorbed ions depends on the metal and on the solution pH (see Table S1 of the Electronic Supplementary material). As can be seen in the table, the most favorable Cd^{2+} sorption is achieved at pH = 6. Thus, the isotherm of Cd^{2+} sorption was measured at this pH.

At very low pH, cadmium is present in solution as free Cd^{2+} ion, but there is also a high concentration of H^+ ions that protonate the surface of the material causing a strong positive charge, which blocks the sorption of cadmium ion by electrostatic repulsion. From moderately acidic to neutral conditions, cadmium still exists mostly as free ion, but the competition effect with H^+ markedly decreases.

The effect of the solutions pH on the removal efficiencies of lead can also be explained by the metal speciation at different pH values [34] and the variation in the surface charge of the nanomaterial with pH. The pH for performing the batch sorption experiments with Pb^{2+} was 3. At this pH (Q = 0.195 mmol Pb^{2+}/g NPNH2). Lower pH values were avoided because of the competition effect with H^+, whereas at higher pH precipitation of the hydroxide from the solutions of higher metal concentration takes place (Ksp $Pb(OH)_2 = 1.43 \times 10^{-20}$) [35]. Higher pH values were also avoided because at Pb^{2+} initial concentrations of 100 ppm there is precipitation at pH ⩾ 5 (see Table S1 of the Electronic Supplementary material), and even higher concentrations of Pb^{2+} were employed for obtaining the isotherm.

To further characterize the Pb^{2+} (pH = 3) and Cd^{2+} (pH = 6) sorptions on NPNH2, the isotherms shown in Fig. 5(a and b) were obtained by incubation of 1.0 g L^{-1} of the nanoparticles at 25.0 °C in solutions containing different amounts of the cations.

As can be seen in Fig. 5(a), the values of Q (mmol Pb^{2+}/g NPNH2) linearly increase with the equilibrium concentration (C_{eq}) of Pb^{2+} expressed in mmol L^{-1} (Eq. (2)).

$$Q = (-8.2 \pm 8.7) \times 10^{-3} + (0.22 \pm 0.01) \times C_{eq} \quad (2)$$

The isotherm corresponds to the simplest type of adsorption [36].

For Cd^{2+} the values of Q (mmol Cd^{2+}/g NPNH2) do not increase linearly with C_{eq}, as shown in Fig. 5(b). The data can be fitted to a Freundlich Eq. (3).

$$Q = (5.3 \pm 0.2) \times 10^{-2} \times C_{eq}^{(0.54 \pm 0.05)} \quad (3)$$

where Q and C_{eq} are expressed in mmol Cd^{2+}/g NPNH2 and mmol Cd^{2+} L^{-1}, respectively.

The data can be fitted to the Freundlich isotherm probably because there are at least two different sorption sites with dissimilar affinity [36]. Although these sites could also be available for the adsorption of Pb^{2+}, it seems possible that even higher amounts of this metal would be necessary for observing a deviation from linearity in Fig. 5(a).

The Cd^{2+} adsorption data can also be fitted to a Langmuir isotherm (Eq. (4)).

$$Q = \frac{(0.13 \pm 0.01) \times C_{eq}}{1 + (1.4 \pm 0.3) \times C_{eq}} \quad (4)$$

where Q and C_{eq} are expressed in mmol Cd^{2+}/g NPNH2 and mmol Cd^{2+} L^{-1}, respectively.

Langmuir sorption isotherms are characterized by saturation at high concentrations. From the parameters of Eq. (4), it can be estimated a quantitative value of monolayer for the Langmuir model, which represents the maximum sorption that corresponds to a monolayer Q_{mon} formation of 0.093 mmol of sorbed Cd^{2+} per gram of nanoparticles. This value is lower than the 0.44 mmole of the organic groups in 1 g NPNH2 calculated from the measured %OG, which indicates that not all the amine groups are available for adsorption due to aggregation of the particles.

Comparison of the metals uptake capacity shows that NPNH2 are much better sorbents of Pb^{2+} than of Cd^{2+}. This result is in line with reported data by Aguado et al. for different silica amino-functionalized SBA-15 materials employed to remove heavy metals from water [5] and is also supported by our DFT calculations (see below).

3.3. EXAFS Analysis of the Nano-sorbents

After Pb^{2+} sorption experiments, the suspensions were filtered with 0.1 μm nylon filters and the nanoparticles were gently washed with water, in order to confirm the complexation of the this cation with the silica nanoparticles. Separation of 7 nm diameter particles with this filter is possible due to aggregation of the nanoparticles during the filtering process as already observed for other particles prepared by modification of 7 nm silica particles [7]. EXAFS experiments were performed at the Pb L_3 edge, to provide information of the atomic structure around the sorbent atoms. Thus, it is possible to obtain information on type, number and distances between Pb^{2+} ions and their neighbors and reconstruct the atomic moiety around them. From the X-ray fluorescence spectra it was not possible to detect the presence of lead in bare silica nanoparticles previously incubated with these metal ions, which indicates that upon washing the samples with water, complete removal of the metal occurred. This indicates that lead sorption by silanol groups (if any) should be of physical nature.

The EXAFS oscillation and the corresponding Fourier Transform as well as the fitting function obtained from the NPNH2 sample are shown in Fig. 6. Three shells around Pb^{2+} ions were proposed in the fit and the results are shown in Table 2. Distances longer than 3.5 Å could not be fitted accurately, probably because of the superposition of single and multiple scattering paths. The first fitted shell corresponds to one N atom at 2.28 Å, and the other two correspond to two C atoms at 2.73 and 3.38 Å respectively. This is compatible

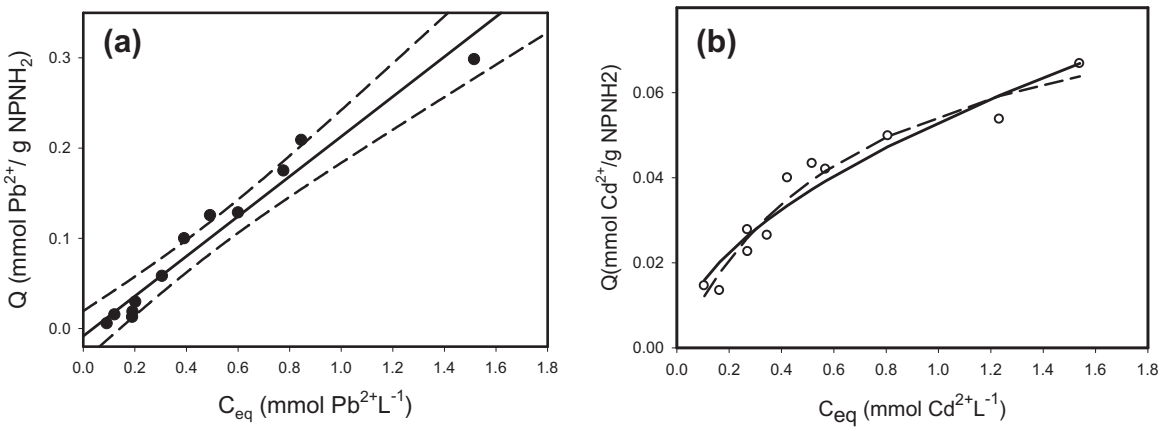

Fig. 5. Plot of Q as a function of the equilibrium concentration of the metal ions obtained by incubation at 25 °C of 1.0 g L^{-1} NPNH2 with solutions of Pb^{2+} at pH = 3 (a) and Cd^{2+} at pH = 6 (b). The 99% confidence interval is shown as dashed lines. The solid and dashed lines in Fig. 4(b) show fitting of the data to Eqs. (3) and (4), respectively.

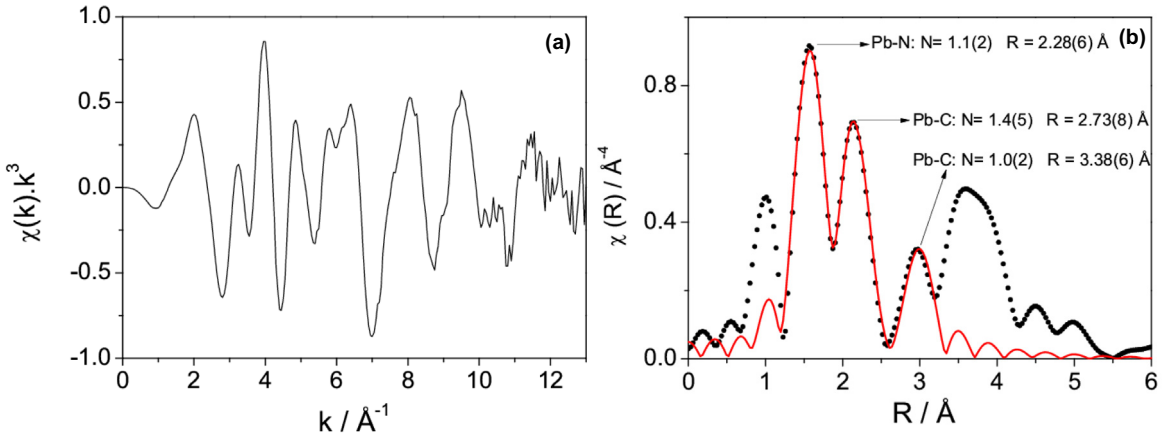

Fig. 6. (a) Pb L_3 edge EXAFS oscillation. (b) Fourier transform of the EXAFS oscillation (filled circles) and the obtained fit (solid line). Errors are given in parentheses.

Table 2
Results obtained for the fits of the Pb L_3 edge EXAFS. *N*: Average coordination number, *R*: interatomic distance, σ^2: Debye–Waller factor. Errors are given in parentheses.

Atom type	*N*	*R* (Å)	σ^2 (Å^2)
N	1.1 (2)	2.28 (6)	0.0037(5)
C	1.4 (5)	2.73 (8)	0.0069(8)
C	1.0 (2)	3.38 (6)	0.0035(6)

with the chemical sorption of Pb^{+2} on N sites of the aminopropyl groups. The second and third neighbors of Pb atoms correspond to the first two C atoms of the chain. Further neighbors observed in the Fourier Transform after 3.2 Å can be associated to single and multiple scattering of the rest of the carbons chain causing a focusing effect because of the linear atoms alignment [37].

3.4. DFT calculations

To compare predicted Pb–N and Pb–C distances in the modified nanoparticles bonded to Pb^{2+} with the EXAFS determinations, DFT calculations were performed. For simplicity, we assumed that the above mentioned interatomic distances in the APTES–Pb^{2+} moiety are only slightly affected by the nanoparticle presence. Therefore, the single APTES–Pb^{2+} molecule has been modeled. The obtained fully optimized structures and the derived relevant data are shown in Fig. 7.

The theoretical Pb–N bond distance of 2.33 Å resulting for the configuration (a) compares well with the experimental one of 2.28 Å, while the predictions for the Pb–C non-bonded distances are in reasonable agreement with the experimental values listed in Table 2. In addition, the calculations indicate that the larger Pb–C distance corresponds to the C atom linked to the N atom.

The cyclic-conformer (b) is much more stable than the conformer (a). In fact, the calculated CPCM-B3LYP/CEP-121G enthalpy change at 298 K for the APTES + Pb^{+2} → APTES–Pb^{+2} association process is −51.3 kcal mol^{-1} for conformer (a) and −80.7 kcal mol^{-1} for conformer (b). On the other hand, enthalpy changes of −45.7 and −78.5 kcal mol^{-1} were estimated for these processes at the CPCM-M06-2X/CEP-121G level of theory. Although the Pb–N and Pb–C interatomic distances in the conformer (b) (Fig. 7(b)) are also consistent with the experimental results, due to the important rearrangement involved (the minimum Pb–O distance in (a) is 5.3 Å, whereas in the cyclic conformer (b) it is only 2.27 Å), it is expected that the cyclization reaction (a) → (b) or the direct insertion reaction of the Pb^{2+} into APTES involves large activation energy values. This assumption is quite consistent with the absence of the EXAFS signal corresponding to the strong Pb–O bond at 2.27 Å.

Similar considerations are expected for the APTES–Cd^{2+} complexes. The corresponding open and cyclic molecular configurations are depicted in Fig. S2 of the Electronic Supplementary material. However, the second conformation is only

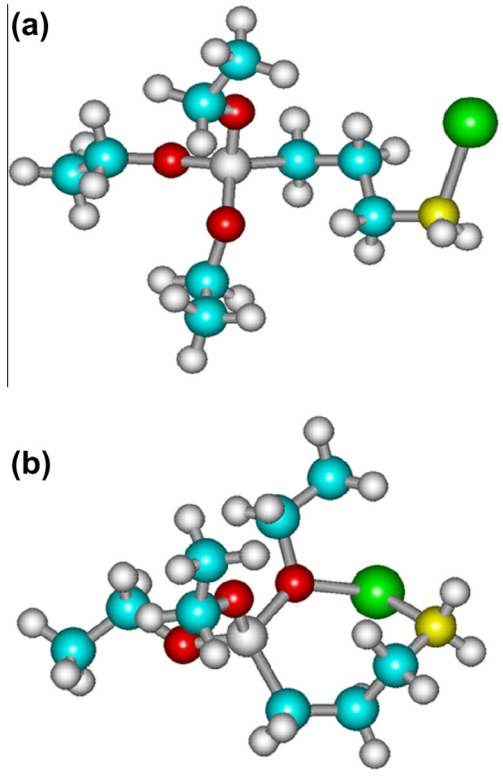

Fig. 7. Optimized structures of APTES–Pb^{2+}, (a) open-conformer and (b) cyclic-conformer, at the CPCM-B3LYP/CEP-121G level of theory. Interatomic distances in Å. Experimental distances obtained by EXAFS are shown in parentheses.

−3.0 kcal mol^{-1} (B3LYP) or −4.6 kcal mol^{-1} (M06-2X) more stable than the first ones. Besides, the enthalpy changes for the formation of the open conformer of APTES–Cd^{2+} of −21.6 kcal mol^{-1} (B3LYP) and −22.3 kcal mol^{-1} (M06-2X) are smaller than the obtained for the open configuration of APTES–Pb^{+2}. These results are in qualitative agreement with the observed much higher sorbent efficiency of APTES for Pb^{2+} than for Cd^{2+}.

3.5. Hybrid NPNH2@MEH-PPV nanoparticles

TEM images for NPNH2@MEH-PPV hybrid particles obtained are shown in Fig. 1(b) (inset). As observed in Fig. 1(b) rapid injection of a THF solution of MEH-PPV dissolved into the aqueous suspension of NPNH2 gave average diameter particles of 300 nm. Similar results were obtained with the suspension of NPNH2 incubated in the Cd^{2+} solution. The procedure can be applied to the separation and removal of nanoparticles employed for the sorption of metal ions, as exemplified here.

4. Conclusion

Silica nanoparticles of 7 nm diameter were modified with (3-aminopropyl) triethoxysilane (APTES) and characterized by CP-MAS ^{13}C and ^{29}Si NMR, FTIR, zeta potential measurements, and thermogravimetry. Isotherms for the adsorption of divalent lead and cadmium ions from aqueous solution were obtained. Lead complexation with these silica nanoparticles was clearly confirmed by EXAFS. Predicted Pb–N and Pb–C distances obtained from quantum-chemical calculations are in very good agreement with the EXAFS determinations. The calculations also support the higher APTES affinity for Pb^{2+} compared to Cd^{2+}. A novel method to facilitate the separation of small organofunctionalized nanoparticles from the aqueous medium, consisting in preparing multiphase particles of the copolymer poly[2-methoxy-5-(2-ethylhexyl-oxy)-1,4-phenylene-vinylene] and the modified silica nanoparticles was also proposed.

Acknowledgments

This work was supported by Grant PICT 2008 # 0686 from Agencia Nacional de Promoción Científica y Tecnológica, (ANPCyT, Argentina), PIP # 01035 (CONICET, Argentina) and LNLS (Brasil, Project XAFS1-14534). M.M., J.M.R.L., C.J.C. and E.R.D. are researchers from CONICET. V.B.A. and D.O.M. are researchers from Comisión de Investigaciones Científicas de la Provincia de Buenos Aires.

The authors thank Drs. J.C. Combo and C. Bilos from LAQAB (Universidad Nacional de La Plata) for the nitrogen determination.

Appendix A. Supplementary data

Supplementary data associated with this article can be found, in the online version, at http://dx.doi.org/10.1016/j.saa.2015.06.093.

References

[1] Directive 2013/39/EC of the European Parliament and of the Council of 12 August 2013 amending directives 2000/60/EC and 2008/105/EC as regards priority substances in the field of water policy.
[2] A. Dabrowski, Z. Hubicki, P. Podkościelny, E. Robens, Selective removal of the heavy metal ions from waters and industrial wastewaters by ion-exchange method, Chemosphere 56 (2007) 91–106.
[3] US EPA, Hazardous Waste Treatment, Storage, and Disposal Facilities (TSDF) Regulations (2014), EPA 530-R-11-006 Version 4, USA. <http://www.epa.gov>.
[4] L. Carlos, F.S. García Einschlag, M.C. Gonzalez, D.O. Mártire, Applications of magnetite nanoparticles for heavy metal removal from wastewater, in: F.S. García Einschlag, L. Carlos (Eds.), Waste Water – Treatment Technologies and Recent Analytical Developments, In Tech, Rijeka, 2013, pp. 64–77.
[5] J. Aguado, J.M. Arsuaga, A. Arencibia, M. Lindo, V. Gascón, Aqueous heavy metals removal by adsorption on amine-functionalized mesoporous silica, J. Hazard. Mat. 163 (2009) 213–221.
[6] J.L. Foschiera, T.M. Pizzolato, E.V. Benvenutti, FTIR thermal analysis on organofunctionalized silica gel, J. Braz. Chem. Soc. 12 (2001) 159–164.
[7] V.B. Arce, S.G. Bertolotti, F.J.V.E. Oliveira, C. Airoldi, M.C. Gonzalez, P.E. Allegretti, D.O. Mártire, Safranine-T triplet-state quenching by modified silica nanoparticles, J. Phys. Chem. C 115 (2011) 18122–18130.
[8] V.B. Arce, J. Scotto, P.E. Allegretti, M.A. Melo Jr., C. Airoldi, M.L. Salum, R. Erra-Balsells, R. Pis Diez, D.O. Mártire, A combined experimental and computational investigation of the fluorescence quenching of riboflavin by cinnamic alcohol chemisorbed on silica nanoparticles, J. Phys. Chem. C 118 (2014) 15348–15355.
[9] C. Wu, C. Szymanski, J. McNeill, Preparation and encapsulation of highly fluorescent conjugated polymer nanoparticles, Langmuir 22 (2006) 2956–2960.
[10] J. Pecher, S. Mecking, Nanoparticles of conjugated polymers, Chem. Rev. 110 (2010) 6260–6279.
[11] B. Ravel, M. Newville, ATHENA, ARTEMIS, HEPHAESTUS: data analysis for X-ray absorption spectroscopy using IFEFFIT, J. Synchrotron. Rad. 12 (2005) 537–541.
[12] S.I. Zabinski, J.J. Rehr, A. Ankudinov, R.C. Albers, M.J. Eller, Multiple-scattering calculations of X-ray-absorption spectra, Phys. Rev. B 52 (1995) 2995–3009.
[13] A.D. Becke, Density-functional thermochemistry. iii. The role of exact exchange, J. Chem. Phys. 98 (1993) 5648–5652.
[14] A.D. Becke, Density-functional exchange-energy approximation with correct asymptotic behavior, Phys. Rev. A 38 (1988) 3098–3100.
[15] C. Lee, W. Yang, R.G. Parr, Development of the Colle–Salvetti correlation-energy formula into a functional of the electron density, Phys. Rev. B 37 (1988) 785–789.
[16] Y. Zhao, D.G. Truhlar, The M06 suite of density functionals for main group thermochemistry, thermochemical kinetics, noncovalent interactions, excited states, and transition elements: two new functionals and systematic testing of four M06-class functionals and 12 other functionals, Theor. Chem. Acc. 120 (2008) 215–241.
[17] W.J. Stevens, H. Basch, M. Krauss, Compact effective potentials and efficient shared-exponent basis sets for the first- and second-row atoms, J. Chem. Phys. 81 (1984) 6026–6033.
[18] W.J. Stevens, M. Krauss, H. Basch, P.G. Jasien, Relativistic compact effective potentials and efficient, shared-exponent basis sets for the third-, fourth-, and fifth-row atoms, Can. J. Chem. 70 (1992) 612–630.
[19] V. Barone, M. Cossi, Quantum calculation of molecular energies and energy gradients in solution by a conductor solvent model, J. Phys. Chem. A 102 (1998) 1995–2001.

[20] M.J. Frisch et al., Gaussian 09, Revision A.02, Gaussian Inc, Wallingford, CT, 2009.
[21] A.E. Ruiz, P. Caregnato, V.B. Arce, M.M. Schiavoni, V.C. Mora, M.C. Gonzalez, P.E. Allegretti, D.O. Mártire, Synthesis and characterization of butoxylated silica nanoparticles. Reaction with benzophenone triplet-states, J. Phys. Chem. C 111 (2007) 7623–7628.
[22] M.J. Llansola Portolés, F. Rodríguez Nieto, D.B. Soria, J.I. Amalvy, P.J. Peruzzo, D.O. Mártire, M.O. Kotler, O. Holub, M.C. Gonzalez, Photophysical properties of blue-emitting silicon nanoparticles, J. Phys. Chem. C 113 (2009) 13694–13702.
[23] E.T. Vandenberg, L. Bertilsson, B. Liedberg, K. Uvdal, R. Erlandsson, H. Elwing, I. Lundström, Structure of 3-aminopropyl triethoxy silane on silicon oxide, J. Colloid Interface Sci. 147 (1991) 103–118.
[24] J. Coates, Interpretation of infrared spectra. A practical approach, John Coates, in: R.A. Meyers (Ed.), Encyclopedia of Analytical Chemistry, John Wiley & Sons Ltd, Chichester, 2000, pp. 10815–10837.
[25] J.J. Romero, M.J. Llansola Portolés, M.L. Dell'Arciprete, H.B. Rodriguez, A.L. Moore, M.C. Gonzalez, Photoluminiscent 1–2 nm sized silicon nanoparticles: a surface-dependent system, Chem. Mater. 25 (2013) 3488–3498.
[26] E. Kaiser, R.L. Colescott, C.D. Bossinger, P.I. Cook, Color test for detection of free terminal amino groups in the solid-phase synthesis of peptides, Anal. Biochem. 34 (1970) 595–598.
[27] A.S.O. Moscofian, C.T.G.V.M.T. Pires, A.P. Vieira, C. Airoldi, Removal of reactive dyes using organofunctionalized mesoporous silicas, J. Porous Mater. 20 (2013) 1179–1188.
[28] C.R. Silva, I.C.S.F. Jardim, C. Airoldi, New stationary phase prepared by immobilization of a copper amine complex on silica and its use for high performance liquid chromatograph, J. High Resol. Chromatogr. 22 (1999) 103–108.
[29] T. Yokoi, H. Yoshitake, T. Yamada, Y. Kubota, T. Tatsumi, Amino-functionalized mesoporous silica synthesized by a novel synthesis route using an anionic surfactant, J. Mater. Chem. 16 (2006) 1125–1135.
[30] M.A. Melo Jr., F.J.V.E. Oliveira, J.A.A. Sales, C. Airoldi, Useful aminoalcohol molecules incorporated in an epoxide silylating agent for silica organofunctionalization and thermodynamics of copper removal, New J. Chem. 33 (2009) 1038–1046.
[31] P. Wilhelm, D. Stephan, On-line tracking of the coating of nanoscaled silica with titania nanoparticles via zeta-potential measurements, J. Colloid Interface Sci. 293 (2006) 88–92.
[32] Z. Csőgör, M. Nacken, M. Sameti, C.M. Lehr, H. Schmidt, Modified silica particles for gene delivery, Mater. Sci. Eng., C 23 (2003) 93–97.
[33] A.E. Martell, R.M. Smith, Critical Stability Constants, vol. 1–4, Plenum Press, New York, 1976.
[34] K.J. Powell, P.L. Brown, R.H. Byrne, T. Gajda, G. Hefter, A. Leuz, S. Sjöberg, H. Wanner, Chemical speciation of environmentally significant metals with inorganic ligands. Part 3: The Pb^{2+} + OH^-, Cl^-, CO_3^{2-}, SO_4^{2-}, and PO_4^{3-} systems (IUPAC Technical Report), Pure Appl. Chem. 81 (2009) 2425–2476.
[35] Q. Liu, Y. Liu, Distribution of Pb(II) species in aqueous solutions, J. Colloid Interface Sci. 268 (2003) 266–269.
[36] H.-J. Butt, K. Graf, M. Kappl, Physics and Chemistry of Interfaces, first ed., Wiley-VCH, Weinheim, 2003.
[37] E. Stern, Theory of EXAFS, in: D.C. Konisberger, R. Prins (Eds.), X-ray Absorption Principles, Applications, Techniques of EXAFS, SEXAFS and XANES, John Wiley and Sons, 1988, pp. 34–36.

Spectrochimica Acta Part A: Molecular and Biomolecular Spectroscopy xxx (2015) xxx–xxx

Contents lists available at ScienceDirect

Spectrochimica Acta Part A: Molecular and Biomolecular Spectroscopy

journal homepage: www.elsevier.com/locate/saa

Corrigendum

Corrigendum to "EXAFS and DFT study of the cadmium and lead adsorption on modified silica nanoparticles" [Spectrochim. Acta Part A: Mol. Biomol. Spectrosc. 151 (2015) 156–163]

Valeria B. Arce [a,b], Romina M. Gargarello [a], Florencia Ortega [a], Virginia Romañano [a], Martín Mizrahi [a], José M. Ramallo-López [a], Carlos J. Cobos [a], Claudio Airoldi [c], Cecilia Bernardelli [d], Edgardo R. Donati [d], Daniel O. Mártire [a,*]

[a] Instituto de Investigaciones Fisicoquímicas Teóricas y Aplicadas (INIFTA), CCT-La Plata-CONICET, Universidad Nacional de La Plata, Diag 113 y 64, 1900 La Plata, Argentina
[b] Centro de Investigaciones Ópticas (CIOp), CONICET La Plata-CIC, CC 3, 1897 Gonnet, La Plata, Argentina
[c] Chemistry Institute, University of Campinas, P.O. Box 6154, 13084-971 Campinas, São Paulo, Brazil
[d] Centro de Investigación y Desarrollo en Fermentaciones Industriales, CINDEFI (CCT La Plata-CONICET, Universidad Nacional de La Plata), Facultad de Ciencias Exactas, 50 y 115, 1900 La Plata, Argentina

The authors regret to inform that in Fig. 7 of this article some information was missing. The corrected Fig. 7 is shown below. Authors would like to apologize for the inconvenience caused.

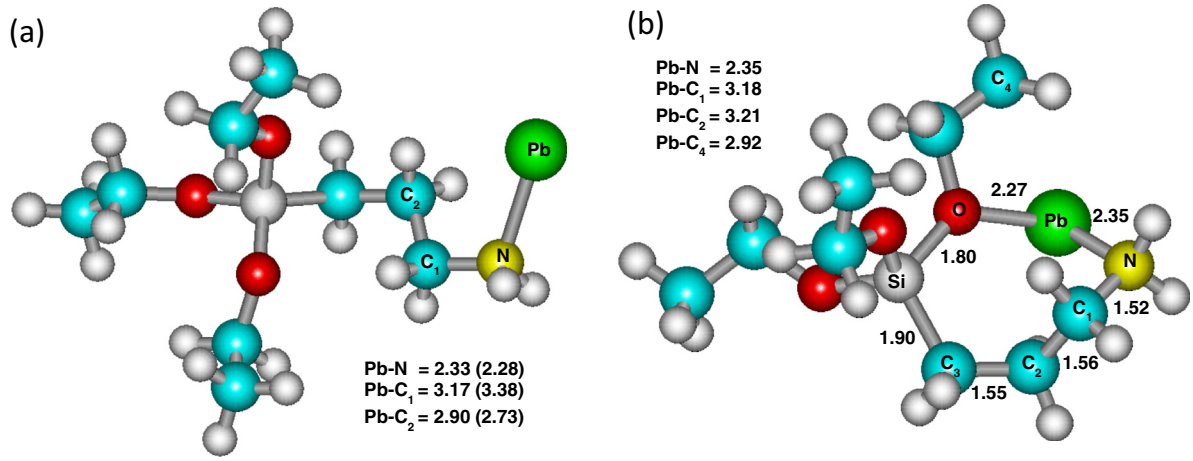

Fig. 7. Optimized structures of APTES-Pb^{2+}, (a) open-conformer and (b) cyclic-conformer, at the CPCM-B3LYP/CEP-121G level of theory. Interatomic distances in Å. Experimental distances obtained by EXAFS are shown in parentheses.

DOI of original article: http://dx.doi.org/10.1016/j.saa.2015.06.093
* Corresponding author. Tel.: +54 221 4257430; fax: +54 221 4254642.
E-mail addresses: danielmartire@gmail.com, dmartire@inifta.unlp.edu.ar (D.O. Mártire).

http://dx.doi.org/10.1016/j.saa.2015.07.026
1386-1425/